Spectroscopy and 2.8 μm laser operation of disordered Er:CLNGG crystals

Simone Normani, Pavel Loiko, Zhongben Pan, Elena Dunina, Liudmila Fomicheva, Alexey Kornienko, Alain Braud, Weidong Chen, Uwe Griebner, Valentin Petrov, et al.

Spectroscopy and 2.8 µm laser operation of disordered Er:CLNGG crystals

Simone Normani,[1] Pavel Loiko,[1] Zhongben Pan,[2] Elena Dunina,[3] Liudmila Fomicheva,[4] Alexey Kornienko,[3] Alain Braud,[1] Weidong Chen,[5] Uwe Griebner,[5] Valentin Petrov,[5] and Patrice Camy[1,*]

[1]*Centre de Recherche sur les Ions, les Matériaux et la Photonique (CIMAP), UMR 6252 CEA-CNRS-ENSICAEN, Université de Caen Normandie, 6 Boulevar Maréchal Juin, 14050 Caen Cedex 4, France*
[2]*School of Information Science and Engineering, Shandong University, 72 Binhai Road, Qingdao 266237, China*
[3]*Vitebsk State Technological University, 72 Moskovskaya Ave., 210035 Vitebsk, Belarus*
[4]*Belarusian State University of Informatics and Radioelectronics, 6 Brovka St., 220027 Minsk, Belarus*
[5]*Max Born Institute for Nonlinear Optics and Short Pulse Spectroscopy, Max-Born-Str. 2a, 12489 Berlin, Germany*
**Corresponding author: patrice camy@ensicaen.fr*

Received XX Month XXXX; revised XX Month, XXXX; accepted XX Month XXXX; posted XX Month XXXX (Doc. ID XXXXX); published XX Month XXXX

We report on the first laser operation on the $^4I_{11/2}$→$^4I_{13/2}$ transition of erbium-doped disordered calcium lithium niobium gallium garnet (CLNGG) crystals with broadband mid-infrared emission properties. A 41.4 at.% Er:CLNGG continuous-wave laser generated 292 mW at 2.80 µm with 23.3% slope efficiency and a laser threshold of 209 mW. Er^{3+} ions in CLNGG feature inhomogeneously broadened spectral bands (σ_{SE} = 1.79×10^{-21} cm^2 at 2.79 µm, emission bandwidth: 27.5 nm), large luminescence branching ratio for the $^4I_{11/2}$ → $^4I_{13/2}$ transition of 17.9%, and a favorable ratio of the $^4I_{11/2}$ and $^4I_{13/2}$ lifetimes exhibiting values of 0.34 ms and 1.17 ms (for 41.4 at.% Er^{3+}), respectively. © 2023 Optical Society of America

http://dx.doi.org/10.1364/OL.99.099999

Calcium lithium niobium gallium garnet (CLNGG) is a disordered crystal belonging to the family of cubic multicomponent garnets (sp. gr. *Ia*$\bar{3}$*d*) [1]. CLNGG is an attractive laser host material for doping with rare-earth ions such as Nd^{3+}, Yb^{3+}, Tm^{3+}, or Ho^{3+} replacing for the Ca^{2+} cations in dodecahedral (D_2) sites with VIII-fold oxygen coordination [2-5]. The structure disorder in CLNGG originates from a random distribution of Ga^{3+} and Nb^{5+} cations over two non-equivalent (octahedral and tetrahedral) lattice sites with Li^+ playing the role of a local charge compensator [6], Fig. 1(a). This leads to a variation of composition of the multi-ligands in the vicinity of the dopant ions and a significant inhomogeneous spectral broadening. The broadband emission properties of rare-earth-doped CLNGG crystals are very appealing for applications in tunable and mode-locked lasers [2-5].

Erbium ions (Er^{3+}) attract attention because of their mid-infrared emission at ~3 µm. It originates from the $^4I_{11/2} \longrightarrow {}^4I_{13/2}$ transition having a self-terminating nature [7]. The bottleneck effect owing to a longer luminescence lifetime of the terminal laser level can be avoided at high Er^{3+} doping levels due to an energy-transfer upconversion (ETU) process, $^4I_{13/2} + {}^4I_{13/2} \rightarrow {}^4I_{15/2} + {}^4I_{9/2}$, emptying the terminal laser level [8]. The ETU rate depends quadratically on the doping level. In this way, continuous-wave (CW) laser operation on the $^4I_{11/2} \rightarrow {}^4I_{13/2}$ transition becomes feasible.

Among the gain media for 3 µm lasers, heavily Er^{3+}-doped cubic garnets such as $Y_3Sc_2Ga_3O_{12}$ (YSGG), $Gd_3Ga_5O_{12}$ (GGG) or $Y_3Al_5O_{12}$ (YAG), are popular despite their high phonon energies [9-11]. They can be grown by the Czochralski method, combine good thermo-mechanical properties of the host matrix and suitable spectroscopic behavior of the dopant Er^{3+} ions, such as a reasonable $^4I_{11/2}$ to $^4I_{13/2}$ luminescence lifetime ratio, a strong ETU and a strong crystal-field allowing for long emission wavelengths well addressing specific applications. Mid-infrared Er:YAG lasers are widely used in painless monitoring of blood sugar levels, laser treatment of soft tissues and dentistry [12]. In particular, the laser emission at 2.8 µm well matches the absorption of hydroxyapatite in hard body tissues.

Disordered laser crystals are essential for the design of broadly tunable lasers, e.g., with variable penetration depth into biological tissues. Unfortunately, the $^4I_{11/2} \longrightarrow {}^4I_{13/2}$ emission spectra of Er:YAG and Er:YSGG crystals contain a set of sharp peaks defining the accessible laser lines [13]. It is relevant to develop crystalline laser materials with a "glassy-like" spectroscopic behavior (smooth and broad emission spectra). Broadband emission in this spectral range can also be achieved with Cr^{2+}-doped ZnSe and CdSe crystals.

In the present work, we report on the spectroscopic properties and 2.8 µm laser operation of heavily Er^{3+}-doped disordered CLNGG garnet crystals with broadband emission properties.

The crystals of Er:CLNGG were grown by the Czochralski method using Pt crucibles under 90% Ar + 10% CO_2 atmosphere. The raw materials were $CaCO_3$, Nb_2O_5 (purity: 4N), Ga_2O_3, Er_2O_3 and Li_2CO_3 (5N). The initial Er^{3+} doping levels were 10 at.% and 30 at.% (with respect to Ca^{2+}). An excess of 1.5 wt.% Ga_2O_3 was added. The polycrystalline garnet phase was obtained by a solid-state reaction at 1200 °C. A [111] oriented undoped CLNGG seed was used. The pulling rate was 0.6 – 2 mm/h and the rotation speed was 11 rpm. After the growth was completed, the crystal was cooled down to room temperature (RT, 293 K) at a rate of 10 – 20 °C/h. The as-grown crystals (Φ = 25 mm, length: 55 mm) were annealed in air at

1100 °C for 48 h. The annealed crystals were transparent and rose-colored due to Er^{3+} doping, Fig. 1(b). The actual Er^{3+} doping level was measured by Inductively Coupled Plasma-Optical Emission Spectroscopy yielding 14.7 at.% and 41.4 at.% (ion density: N_{Er} = 1.92 and 6.21×10^{21} at/cm^3, respectively). The crystal structure (cubic, sp. gr. O^{10}_h - $I\bar{a}3d$) was confirmed by X-ray diffraction. The thermal conductivity of the 41.4 at.% Er^{3+}-doped crystal was measured by the laser flash method yielding 3.0 Wm^{-1}K^{-1} at RT.

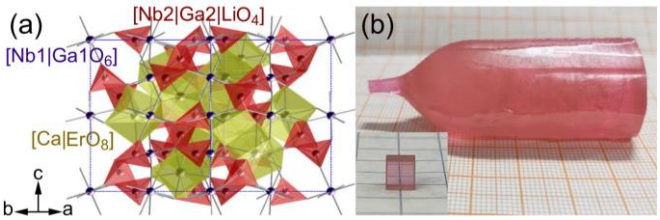

Fig. 1. Er:CLNGG crystals: (a) a fragment of the crystal structure; (b) a photograph of an air annealed 41.4 at.% Er:CLNGG crystal, the growth direction is along the [111] axis, *inset* – polished sample.

The absorption cross-sections, σ_{abs}, Er^{3+} ions in CLNGG are shown in Fig. 2. The electric dipole (ED) contributions to 4f – 4f transition intensities of Er^{3+} ions were calculated using a modified Judd-Ofelt theory accounting for an intermediate configuration interaction [14]. The set of squared reduced matrix elements $U^{(k)}$ was calculated using the free-ion parameters from [15]. The magnetic dipole (MD) contributions to transition intensities were calculated within the Russell–Saunders approximation using wave functions under the assumption of a free-ion. The experimental (f_{exp}) and calculated (f_{calc}) absorption oscillator strengths are shown in Fig. 2. The r.m.s. deviation between them is 0.061. The intensity parameters are $\Omega_2 = 2.176, \Omega_4 = 0.849, \Omega_6 = 0.571$ [10^{-20} cm^2], $R_2 = -0.386, R_4 = -0.035$, $R_6 = 0.034$ [10^{-4} cm] (the R_k parameters describe the configuration interaction). The radiative lifetimes for the $^4I_{13/2}$ and $^4I_{11/2}$ states τ_{rad} are 5.66 ms and 5.53 ms, respectively, and luminescence branching ratio $\beta_{JJ'}$ for the $^4I_{11/2} \longrightarrow {}^4I_{13/2}$ transition is 17.9%.

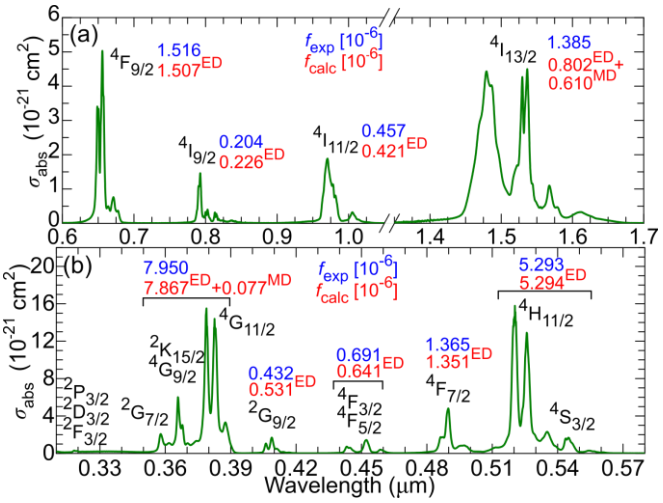

Fig. 2. (a,b) Absorption cross-section, σ_{abs}, spectrum of Er^{3+} ions in the CLNGG crystal: (a) 0.6 – 1.7 μm; (b) 0.31 – 0.58 μm.

The vibronic properties of Er:CLNGG crystals were studied by Raman spectroscopy, Fig. 3(a). The structured high energy bands at 750 / 772 cm^{-1} and 828 / 848 cm^{-1} are assigned to symmetric stretching modes (ν_s) of isolated metal-oxygen tetrahedra [$Ga2O_4$] and [$Nb2O_4$], respectively [16]. The weak shoulder at 848 cm^{-1} which is assigned to cationic vacancies in [$Nb2O_4$] indicates the positive role of Li^+ codoping for the local charge compensation in tetrahedral sites even at very high Er^{3+} doping levels. The maximum phonon energy of Er:CLNGG is 848 cm^{-1}.

The absorption cross-sections, σ_{abs}, for the $^4I_{15/2} \rightarrow {}^4I_{11/2}$ pump transition of Er^{3+} ions in CLNGG are shown in Fig. 3(b). The peak σ_{abs} is 1.88×10^{-21} cm^2 at 970.7 nm and the corresponding absorption bandwidth (full width at half maximum, FWHM) is 14.0 nm. The stimulated-emission (SE) cross-sections, σ_{SE}, for the $^4I_{11/2} \rightarrow {}^4I_{13/2}$ Er^{3+} transition in the mid-infrared spectral range were calculated by the Füchtbauer-Ladenburg formula [17] from the luminescence spectrum corrected for the structured water vapor absorption in the air, see Fig. 3(c). The maximum σ_{SE} is 2.70×10^{-21} cm^2 at 2706 nm (zero-phonon line, ZPL, at RT), and at longer wavelengths, a weaker emission peak appears ($\sigma_{SE} = 1.79\times10^{-21}$ cm^2 at 2790 nm, emission bandwidth: 27.5 nm). The absorption and emission spectra of Er^{3+} ions in CLNGG are smooth and broad reflecting an inhomogeneous spectral broadening due to the structure disorder.

For comparison, we have also studied the absorption and mid-infrared emission properties of the Er:YSGG crystal, a state-of-the-art garnet gain material for ~2.8 μm lasers. This crystal exhibits a local structure disorder (a partial substitution of Ga^{3+} by Sc^{3+} in octahedral sites). Er^{3+} ions in YSGG show narrow intense spectral lines: the maximum σ_{abs} is 4.46×10^{-21} cm^2 at 968.8 nm (FWHM of only 1.9 nm) for the $^4I_{15/2} \rightarrow {}^4I_{11/2}$ transition, and σ_{SE} is 4.66×10^{-21} cm^2 at 2797 nm (emission bandwidth: 7.3 nm) for the $^4I_{11/2} \rightarrow {}^4I_{13/2}$ mid-infrared transition.

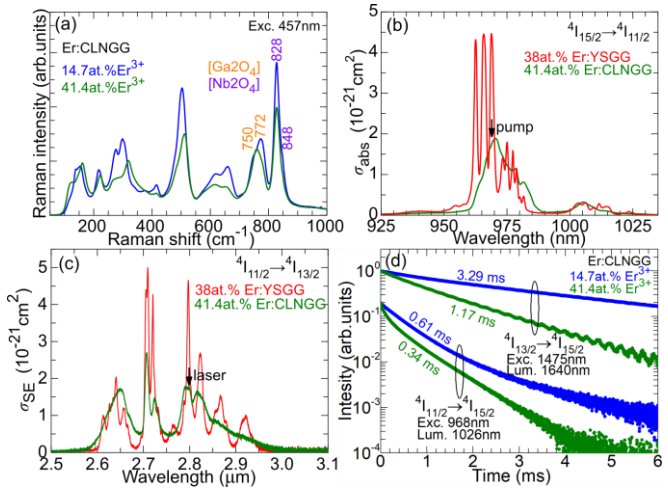

Fig. 3. Spectroscopy of Er^{3+} ions in CLNGG: (a) Raman spectra, *numbers* – peak frequencies in cm^{-1}, $\lambda_{exc} = 457$ nm; (b,c) a comparison of Er:CLNGG and Er:YSGG crystals: (b) absorption cross-sections, σ_{abs}, for the $^4I_{15/2} \rightarrow {}^4I_{11/2}$ transition; (c) SE cross-sections, σ_{SE}, for the $^4I_{11/2} \rightarrow {}^4I_{13/2}$ transition; (d) luminescence decay curves from the $^4I_{11/2}$ and $^4I_{13/2}$ states of Er^{3+} ions in CLNGG measured under resonant excitation.

The luminescence decay from the $^4I_{13/2}$ and $^4I_{11/2}$ states of Er^{3+} ions in CLNGG was studied under resonant excitation using finely

powdered samples to avoid the effect of radiation trapping, see Fig. 3(d). The resulting mean luminescence lifetimes $<\tau_{lum}>$ are 3.29 ms and 0.61 ms (14.7 at.% Er^{3+}) and 1.17 ms and 0.34 ms (41.4 at.% Er^{3+}), respectively. Note that the luminescence lifetimes of the upper laser level ($^4I_{11/2}$) are much shorter than the radiative one (5.53 ms) owing to a non-negligible multiphonon non-radiative relaxation in the high-phonon-energy CLNGG crystal.

The luminescence lifetimes of the $^4I_{11/2}$ and $^4I_{13/2}$ manifolds of Er^{3+} ions in five garnet crystals with a doping level about 30 – 50 at.% are compared in Fig. 4, including CLNGG (this work), YSGG, YAG, GGG [9] and GSGG [18,19]. Although the lifetime of the upper laser level for Er^{3+} ions in CLNGG is relatively short (still being longer than that for YAG), the lifetime of the terminal laser level responsible for the bottleneck effect is the shortest one, leading to a favorable $^4I_{13/2}$ / $^4I_{11/2}$ lifetime ratio.

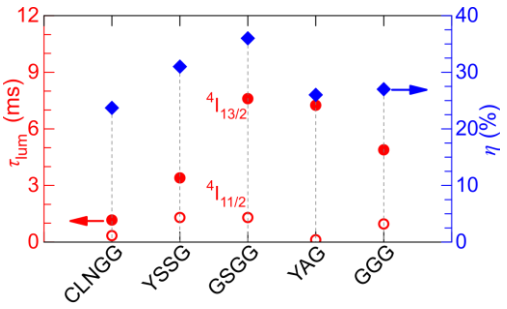

Fig. 4. Comparison of luminescence lifetimes, τ_{lum}, for the upper ($^4I_{13/2}$) and lower ($^4I_{11/2}$) laser levels (*full and open red circles*, respectively) and slope efficiency η for the $^4I_{11/2} \rightarrow {}^4I_{13/2}$ laser transition (*blue diamonds*) for Er^{3+} ions in five garnet crystals: CLNGG (this work), YSGG, YAG, GGG [9] and GSGG [18,19]. Er^{3+} doping level: 30 – 50 at.%.

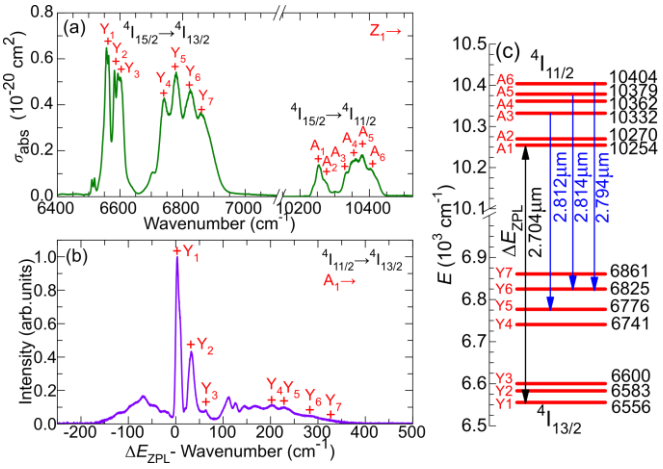

Fig. 5. Low-temperature (12 K) spectroscopy of Er^{3+} ions in CLNGG: (a) absorption spectra, the $^4I_{15/2} \rightarrow {}^4I_{11/2}$ and $^4I_{13/2}$ transitions; (b) emission spectrum, the $^4I_{11/2} \rightarrow {}^4I_{13/2}$ transition; (c) energy sub-level diagram for the $^4I_{11/2}$ and $^4I_{13/2}$ Er^{3+} manifolds. "+"mark electronic transitions, ΔE_{ZPL} – zero-phonon line energy. *Blue arrows* in (c) indicate transitions responsible for the laser emission.

The low-temperature (12 K) absorption and emission spectra of Er^{3+} ions in CLNGG, Fig. 5(a,b), were measured to determine the crystal-field splitting of the upper and lower laser levels, Fig. 5(c). Er^{3+} ions in CLNGG replace for the Ca^{2+} ones in D_2 symmetry sites with an VIII-fold oxygen coordination. Each $^{2S+1}L_J$ multiplet is split into J + 1/2 energy levels. The empirical notations for the $^4I_{15/2}$, $^4I_{13/2}$ and $^4I_{11/2}$ levels were used: Z_i, Y_j and A_k. The spectral bands of Er^{3+} ions in CLNGG at 12 K are inhomogeneously broadened, but all the Stark sub-levels are well resolved. For the $^4I_{11/2} \rightarrow {}^4I_{13/2}$ transition, the zero-phonon line energy for transition between the lowest Stark sub-levels of both multiplets is ΔE_{ZPL} = 3698 cm^{-1} (2.704 μm).

The rectangular laser elements (aperture: 3×3 mm^2, thickness: 3.0-3.5 mm) were cut from annealed 14.7 at.% Er: and 41.4 at.% Er:CLNGG crystals for light propagation along the [111] direction. They were polished on both sides to laser-grade quality with good parallelism and left uncoated. The laser elements were mounted on a Cu-holder. We built a hemispherical cavity formed by a flat pump mirror (PM) coated for high transmission (T = 85.7%) at 0.97 μm and high reflection at 2.6 – 3.0 μm, and a set of concave output couplers (OCs) with a radius of curvature of -100 mm and a transmission T_{OC} in the range of 0.33% - 4% at 2.7 – 2.9 μm. The crystal was placed close to the PM with an air gap of <1 mm, and the cavity length was 99 mm. The pump source was a CW Ti:Sapphire laser delivering up to 3.2 W with $M^2 \approx 1$. For the 14.7 at.% Er-doped crystal, the pump wavelength was ~969 nm, while for the 41.4 at.% Er-doped one, it was detuned from the $^4I_{15/2} \longrightarrow {}^4I_{11/2}$ absorption maximum for more uniform pump distribution across the crystal maximizing the laser output. The pump radiation was focused into the crystal using an antireflection-coated achromatic lens (f = 75 mm) leading to a pump spot diameter of 125 ± 5 μm. The measured single-pass pump absorption was 62.0% / 59.0% for 14.7 at.% Er / 41.4 at.% Er:CLNGG, respectively (accounting for the ground-state bleaching). The residual pump after the OC was filtered out using a long-pass filter. The laser spectra were recorded using a ZrF_4 fiber (Thorlabs) and a spectrum analyzer (Bristol, 771 series).

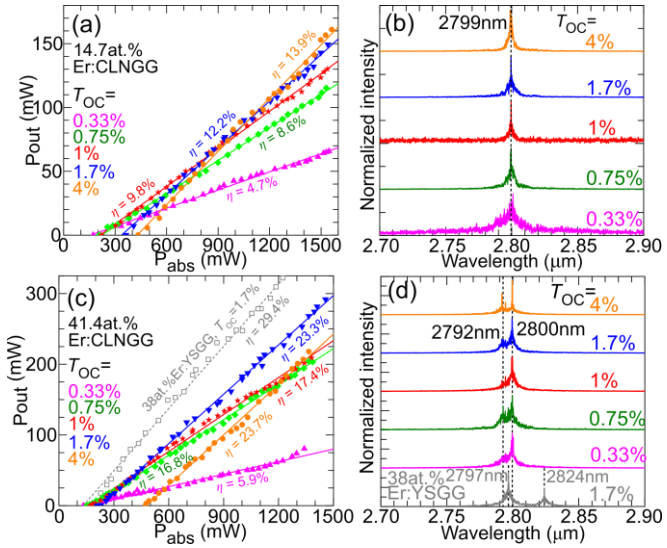

Fig. 6. Mid-infrared Er:CLNGG lasers: Er^{3+} doping level is (a,b) 14.7 at.% and (c,d) 41.4 at.%: (a,c) input-output dependences, η - slope efficiency, (b,d) spectra of laser emission measured well above the laser threshold. In (c,d), the laser results for a 38 at.% Er:YSGG crystal are given for comparison (T_{OC} = 1.7%).

The input-output dependences of Er:CLNGG lasers operating on the $^4I_{11/2} \rightarrow {}^4I_{13/2}$ transition are shown in Fig. 6(a,c). The 41.4 at.% Er:CLNGG laser generated a maximum output power of 292 mW at 2800 nm with a slope efficiency η of 23.3% (vs. the absorbed pump power) and a laser threshold P_{th} of 209 mW (for T_{OC} = 1.7%), see Fig. 6(c). The optical efficiency at the maximum absorbed pump power of 1.46 W was 20.0%. Even higher slope efficiency of 23.7% was achieved for T_{OC} = 4% corresponding to lower output power of 218 mW. With decreasing the output coupling from 4% to 0.33%, P_{th} gradually decreased from 473 to 134 mW. The laser operated on the fundamental transverse mode with a measured $M^2 < 1.1$.

With reducing the Er^{3+} doping level in CLNGG to 14.7 at.%, the laser performance deteriorated due to a less efficient ETU refilling the upper laser level (the ETU rate is quadratically proportional to N_{Er}), Fig. 6(a). The 14.7 at.% Er:CLNGG laser generated 161 mW at 2800 nm with η = 13.9% and a laser threshold of 433 mW (for high T_{OC} = 4%).

For comparison, we have also studied a 38 at.% Er:YSGG crystal, Fig. 6(c), yielding 356 mW at 2797 and 2824 nm with a higher η of 29.4% and a lower laser threshold P_{th} of 143 mW (for T_{OC} = 1.7%).

The typical spectra of laser emission measured well above the laser threshold are shown in Fig. 6(b,d). As expected for a quasi-four -level laser scheme, they were weakly dependent on T_{OC}. The laser always operated at ~2.80 μm, corresponding to the second intense peak in the σ_{SE} spectrum, Fig. 3(c). It is due to two reasons: (i) the reabsorption at the laser wavelength induced by efficient excited-state absorption (ESA) from the long-living lower laser level, $^4I_{13/2} \rightarrow {}^4I_{11/2}$, and (ii) the structured water vapor absorption in air.

The passive losses in the Er:CLNGG crystals were estimated using the Findlay-Clay analysis [20] by plotting the laser threshold P_{th} as a function of -ln(1 – T_{OC}), see Fig. 7. It yielded a round-trip passive loss of 1.0% / 0.86% for 14.7 at.% / 41.4 at.% Er:CLNGG, respectively, being higher than that for 38 at.% Er:YSGG (L = 0.44%).

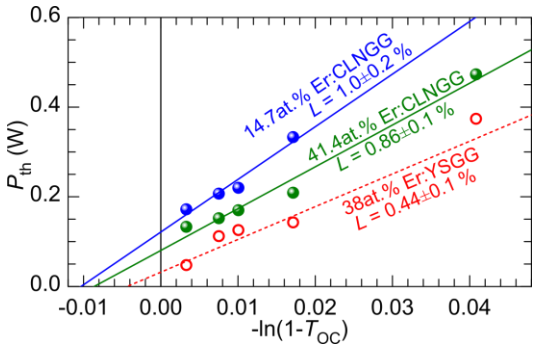

Fig. 7. Estimation of the roundtrip passive losses, L, for Er:CLNGG and Er:YSGG crystals via Findlay-Clay analysis; P_{th} – laser threshold power, T_{OC} – transmission of the output coupler.

To conclude, heavily Er^{3+} doped CLNGG crystals are attractive gain media for mid-infrared lasers operating on the $^4I_{11/2} \rightarrow {}^4I_{13/2}$ transition, due to their broad absorption at 0.97 μm (bandwidth: 14.0 nm) well addressed by commercial high-power InGaAs diode lasers, broad and smooth mid-infrared emission spectra indicating a great potential for broadband wavelength tuning at 2.8 – 3 μm, a relatively large luminescence branching ratio $\beta_{JJ'}$ of 17.9% and a favorable $^4I_{11/2}$ to $^4I_{13/2}$ luminescence lifetime ratio (among garnet crystals). We report on an output power of 292 mW at 2800 nm and a laser slope efficiency up to 23.7% for a 41.4 at.% Er:CLNGG crystal and an evidence of an enhanced ETU for this doping level. Further improvement of the laser efficiency is expected by reducing the passive losses in the crystals via optimizing their growth conditions including the content and type of charge compensators. The power scaling of Er:CLNGG lasers is expected under diode-pumping.

Funding. Agence Nationale de la Recherche (ANR-19-CE08-0028); Région Normandie (Chaire d'excellence "RELANCE"); Contrat de plan État-Région (CPER) de Normandie; National Natural Science Foundation of China (52072351); Qilu Young Scholar Program of Shandong University.

Disclosures. The authors declare no conflicts of interest.

Data availability. Data underlying the results presented in this paper are not publicly available at this time but may be obtained from the authors upon reasonable request.

References

1. M. Y. Young, V. I. Chani, K. Shimamura, and T. Fukuda, J. Cryst. Growth **171**, 463 (1993).
2. Y. Zhang, V. Petrov, U. Griebner, X. Zhang, S. Y. Choi, J. Y. Gwak, F. Rotermund, X. Mateos, H. Yu, H. Zhang, and J. Liu, Opt. Express **22**, 5635 (2014).
3. G. Q. Xie, D. Y. Tang, W. D. Tan, H. Luo, H. J. Zhang, H. H. Yu, and J. Y. Wang, Opt. Lett. **34**, 103 (2009).
4. Y. Wang, Y. Zhao, Z. Pan, J. E. Bae, S. Y. Choi, F. Rotermund, P. Loiko, J. M. Serres, X. Mateos, H. Yu, H. Zhang, M. Mero, U. Griebner, and V. Petrov, Opt. Lett. **43**, 4268 (2018).
5. Y. Zhao, Y. Wang, W. Chen, Z. Pan, L. Wang, X. Dai, H. Yuan, Y. Zhang, H. Cai, J. E. Bae, S. Y. Choi, F. Rotermund, P. Loiko, J. M. Serres, X. Mateos, W. Zhou, D. Shen, U. Griebner, and V. Petrov, Opt. Express **27**, 1922 (2019).
6. M. D. Serrano, J. O. Álvarez-Pérez, C. Zaldo, J. Sanz, I. Sobrados, J. A. Alonso, C. Cascales, M. T. Fernández-Díaz, and A. Jezowski, J. Mater. Chem. C **5**, 11481 (2017).
7. M. Pollnau, Th. Graf, J. E. Balmer, W. Lüthy, and H. P. Weber, Phys. Rev. A. **49**, 3990 (1994).
8. T. Jensen, A. Diening, G. Huber, and B. H. T. Chai, Opt. Lett. **21**, 585 (1996).
9. B. J. Dinerman and P. F. Moulton, Opt. Lett. **19**, 1143 (1994).
10. Z. You, Y. Wang, J. Xu, Z. Zhu, J. Li, H. Wang, and C. Tu, Opt. Lett. **40**, 3846 (2015).
11. E. Arbabzadah, S. Chard, H. Amrania, C. Phillips, and M. Damzen, Opt. Express **19**, 25860 (2011).
12. C. Bader, and I. Krejci, Am. J. Dent. **19**, 178 (2006).
13. P. A. Loiko, E. A. Arbabzadah, M. J. Damzen, X. Mateos, E. B. Dunina, A. A. Kornienko, A. S. Yasukevich, N. A. Skoptsov, and K. V. Yumashev, J. Lumin. **171**, 226 (2016).
14. P. Loiko, A. Volokitina, X. Mateos, E. Dunina, A. Kornienko, E. Vilejshikova, M. Aguiló, and F. Díaz, Opt. Mater. **78**, 495 (2018).
15. P. A. Tanner, V. V. Ravi Kanth Kumar, C. K. Jayasankar, and M. F. Reid. J. Alloy Compd. **215**, 349 (1994).
16. E. Castellano-Hernández, M. D. Serrano, R. J. Jiménez Riobóo, C. Cascales, C. Zaldo, A. Jezowski, and P. A. Loiko, Cryst. Growth Des. **16**, 1480 (2016).
17. B. Aull and H. Jenssen, IEEE J. Quantum Electron. **18**, 925 (1982).
18. D.-L. Sun, J.-Q. Luo, J.-Z. Xiao, Q.-L. Zhang, J.-K. Chen, W.-P. Liu, H.-X. Kang, and S.-T. Yin, Chinese Phys. Lett. **29**, 054209 (2012).
19. R. C. Stoneman and L. Esterowitz, Opt. Lett. **17**, 816 (1992).
20. J. A. Caird, S. A. Payne, P. R. Staver, A. Ramponi, and L. Chase, " IEEE J. Quantum Electron. **24**, 1077 (1988).

Full references

1. M. Y. Young, V. I. Chani, K. Shimamura, and T. Fukuda, “Growth of Ca_3(Li, Nb, Ga)$_5O_{12}$ garnet crystals from stoichiometric melts,” J. Cryst. Growth **171**(3-4), 463-471 (1993).
2. Y. Zhang, V. Petrov, U. Griebner, X. Zhang, S. Y. Choi, J. Y. Gwak, F. Rotermund, X. Mateos, H. Yu, H. Zhang, and J. Liu, "90-fs diode-pumped Yb:CLNGG laser mode-locked using single-walled carbon nanotube saturable absorber," Opt. Express **22**(5), 5635-5640 (2014).
3. G. Q. Xie, D. Y. Tang, W. D. Tan, H. Luo, H. J. Zhang, H. H. Yu, and J. Y. Wang, "Subpicosecond pulse generation from a Nd:CLNGG disordered crystal laser," Opt. Lett. **34**(1), 103-105 (2009).
4. Y. Wang, Y. Zhao, Z. Pan, J. E. Bae, S. Y. Choi, F. Rotermund, P. Loiko, J. M. Serres, X. Mateos, H. Yu, H. Zhang, M. Mero, U. Griebner, and V. Petrov, "78 fs SWCNT-SA mode-locked Tm:CLNGG disordered garnet crystal laser at 2017 nm," Opt. Lett. **43**(17), 4268-4271 (2018).
5. Y. Zhao, Y. Wang, W. Chen, Z. Pan, L. Wang, X. Dai, H. Yuan, Y. Zhang, H. Cai, J. E. Bae, S. Y. Choi, F. Rotermund, P. Loiko, J. M. Serres, X. Mateos, W. Zhou, D. Shen, U. Griebner, and V. Petrov, "67-fs pulse generation from a mode-locked Tm,Ho:CLNGG laser at 2083 nm," Opt. Express **27**(3), 1922-1928 (2019).
6. M. D. Serrano, J. O. Álvarez-Pérez, C. Zaldo, J. Sanz, I. Sobrados, J. A. Alonso, C. Cascales, M. T. Fernández-Díaz, and A. Jezowski, “Design of Yb^{3+} optical bandwidths by crystallographic modification of disordered calcium niobium gallium laser garnets,” J. Mater. Chem. C **5**(44), 11481–11495 (2017).
7. M. Pollnau, Th. Graf, J. E. Balmer, W. Lüthy, and H. P. Weber, “Explanation of the cw operation of the Er^{3+} 3-µm crystal laser,” Phys. Rev. A. **49**(5), 3990-3996 (1994).
8. T. Jensen, A. Diening, G. Huber, and B. H. T. Chai, “Investigation of diode-pumped 2.8-µm Er:$LiYF_4$ lasers with various doping levels”, Opt. Lett. **21**(8), 585-587 (1996).
9. B. J. Dinerman and P. F. Moulton, "3-µm cw laser operations in erbium-doped YSGG, GGG, and YAG," Opt. Lett. **19**(15), 1143-1145 (1994).
10. Z. You, Y. Wang, J. Xu, Z. Zhu, J. Li, H. Wang, and C. Tu, "Single-longitudinal-mode Er:GGG microchip laser operating at 2.7 µm," Opt. Lett. **40**(16), 3846-3849 (2015).
11. E. Arbabzadah, S. Chard, H. Amrania, C. Phillips, and M. Damzen, "Comparison of a diode pumped Er:YSGG and Er:YAG laser in the bounce geometry at the 3 µm transition," Opt. Express **19**(27), 25860-25865 (2011).
12. C. Bader, and I. Krejci, “Indications and limitations of Er: YAG laser applications in dentistry,” Am. J. Dent. **19**(3), 178-86 (2006).
13. P. A. Loiko, E. A. Arbabzadah, M. J. Damzen, X. Mateos, E. B. Dunina, A. A. Kornienko, A. S. Yasukevich, N. A. Skoptsov, and K. V. Yumashev, “Judd-Ofelt analysis and stimulated-emission cross-sections for highly doped (38 at.%) Er:YSGG laser crystal,” J. Lumin. **171**, 226–273 (2016).
14. P. Loiko, A. Volokitina, X. Mateos, E. Dunina, A. Kornienko, E. Vilejshikova, M. Aguiló, and F. Díaz, “Spectroscopy of Tb^{3+} ions in monoclinic $KLu(WO_4)_2$ crystal: Application of an intermediate configuration interaction theory,” Opt. Mater. **78**, 495-501 (2018).
15. P. A. Tanner, V. V. Ravi Kanth Kumar, C. K. Jayasankar, and M. F. Reid. "Analysis of spectral data and comparative energy level parametrizations for Ln^{3+} in cubic elpasolite crystals," J. Alloy Compd. **215**, 349-370 (1994).
16. E. Castellano-Hernández, M. D. Serrano, R. J. Jiménez Riobóo, C. Cascales, C. Zaldo, A. Jezowski, and P. A. Loiko, “Na modification of lanthanide doped $Ca_3Nb1.5Ga3.5O12$-type laser garnets: Czochralski crystal growth and characterization,” Cryst. Growth Des. **16**(3), 1480–1491 (2016).
17. B. Aull and H. Jenssen, “Vibronic interactions in Nd: YAG resulting in nonreciprocity of absorption and stimulated emission cross sections,” IEEE J. Quantum Electron. **18**(5), 925-930 (1982).
18. D.-L. Sun, J.-Q. Luo, J.-Z. Xiao, Q.-L. Zhang, J.-K. Chen, W.-P. Liu, H.-X. Kang, and S.-T. Yin, “Luminescence and thermal properties of Er: GSGG and Yb, Er:GSGG laser crystals,” Chinese Phys. Lett. **29**(5), 054209 (2012).
19. R. C. Stoneman and L. Esterowitz, “Efficient resonantly pumped 2.8-µm Er^{3+}:GSGG laser,” Opt. Lett. **17**(11), 816-818 (1992).
20. J. A. Caird, S. A. Payne, P. R. Staver, A. Ramponi, and L. Chase, "Quantum electronic properties of the $Na_3Ga_2Li_3F_{12}:Cr^{3+}$ laser," IEEE J. Quantum Electron. **24**(6), 1077 - 1099 (1988).